



**4.0%**

Not yet Date: 2022-02-09 05:17 UTC



\* All sources 100 | Internet sources 15 | Publisher sources 3 | Organization archive 6 | Plagiarism Prevention Pool 25

- [0]  dr.ntu.edu.sg/bitstream/10356/40166/3/DasGautomKumar2010.pdf  
1.3% 23 matches


---

- [5]  www.ncbi.nlm.nih.gov/pmc/articles/PMC4644166/  
0.3% 18 matches


---

- [10]  from a PlagScan document dated 2017-10-17 22:01  
0.3% 12 matches  
 1 documents with identical matches



---

- [12]  "Mohamed altaf 3.pdf" dated 2021-05-31  
0.1% 11 matches


---

- [13]  from a PlagScan document dated 2020-06-19 16:19  
0.0% 16 matches


---

- [14]  "Spectroscopic Features Paper-9- August 2020\_Updated.doc" dated 2020-08-10  
0.1% 9 matches  
 1 documents with identical matches

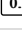
---

- [16]  www.researchgate.net/publication/303801463\_Prussian\_blue\_Type\_Nanoparticles\_for\_Biomedical\_Applications  
0.2% 11 matches

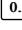
---

- [19]  "AN\_revised\_EHAB paper final LA 16-2-2020\_Final.docx" dated 2020-04-11  
0.5% 7 matches


---

- [25]  "Mohamed Thesis V01.docx" dated 2021-03-27  
0.5% 7 matches


---

- [27]  www.researchgate.net/publication/44692280\_High-relaxivity\_contrast-enhanced\_magnetic\_resonance\_neuroimaging\_A\_review  
0.3% 11 matches

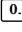
---

- [31]  from a PlagScan document dated 2019-03-22 13:15  
0.1% 10 matches


---

- [35]  "Meera-PHD thesis\_2019.pdf" dated 2019-10-26  
0.0% 7 matches


---

- [37]  from a PlagScan document dated 2020-07-14 02:28  
0.0% 11 matches

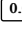
---

- [38]  from a PlagScan document dated 2020-06-14 07:50  
0.2% 8 matches


---

- [44]  macsphere.mcmaster.ca/bitstream/11375/25108/2/Clifford\_Amanda\_M\_2019December\_PhD.pdf  
0.0% 9 matches


---

- [53]  from a PlagScan document dated 2021-10-26 14:34  
0.1% 3 matches

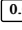
---

- [54]  from a PlagScan document dated 2018-06-14 06:09  
0.2% 6 matches


---

- [57]  www.hindawi.com/journals/mbd/2008/391418/  
0.2% 5 matches


---

- [59]  www.researchgate.net/publication/230721395\_Amine-Functionalized\_Lanthanide-Doped\_Zirconia\_Nanoparticles\_Optical\_Spectroscopy\_Time-Res  
0.5% 4 matches

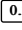
---

- [60]  from a PlagScan document dated 2017-10-26 05:26  
0.0% 7 matches


---

- [61]  from a PlagScan document dated 2017-06-22 14:52  
0.0% 6 matches


---

















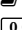



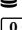
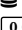
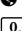
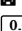
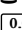
- [65]  from a PlagScan document dated 2019-04-16 20:50  
0.0% 7 matches

---

- [68]  from a PlagScan document dated 2019-02-10 06:08  
0.0% 6 matches

---

- [71]  from a PlagScan document dated 2018-09-30 13:04  
0.0% 5 matches

- 
- [73]  from a PlagScan document dated 2017-09-09 18:56  
 3 matches
- 
- [74]  [www.frontiersin.org/articles/10.3389/fphy.2021.665956/full](http://www.frontiersin.org/articles/10.3389/fphy.2021.665956/full)  
 6 matches
- 
- [75]  from a PlagScan document dated 2018-09-08 15:41  
 3 matches
- 
- [76]  Theranostic nanoparticles based on magnetic nanoparticles: design, preparation, characterization, and evaluation as novel anticancer drug carrier and  
 4 matches
- 
- [77]  Cobalt zinc ferrite nanoparticles as a potential Magnetic Resonance Imaging agent: an in vitro study.(Original Article)(Report)  
 6 matches
- 
- [80]  from a PlagScan document dated 2021-10-24 15:21  
 3 matches
- 
- [83]  from a PlagScan document dated 2018-06-04 08:39  
 3 matches  
 1 documents with identical matches
- 
- [85]  from a PlagScan document dated 2018-02-12 17:37  
 4 matches
- 
- [87]  [www.researchgate.net/publication/254501295\\_Synthesis\\_of\\_biocompatible\\_multicolor\\_luminescent\\_carbon\\_dots\\_for\\_bioimaging\\_applications](http://www.researchgate.net/publication/254501295_Synthesis_of_biocompatible_multicolor_luminescent_carbon_dots_for_bioimaging_applications)  
 5 matches
- 
- [89]  from a PlagScan document dated 2019-07-09 08:41  
 2 matches
- 
- [91]  [www.sciencedirect.com/science/article/pii/S014296120901357X](http://www.sciencedirect.com/science/article/pii/S014296120901357X)  
 1 matches
- 
- [95]  from a PlagScan document dated 2019-03-10 14:38  
 3 matches
- 
- [96]  from a PlagScan document dated 2017-04-03 09:51  
 2 matches
- 
- [97]  [www.researchgate.net/publication/269170583\\_Multi-Modal\\_Imaging\\_And\\_Cancer\\_Therapy\\_Using\\_Lanthanide\\_Oxide\\_Nanoparticles\\_Current\\_Stat](http://www.researchgate.net/publication/269170583_Multi-Modal_Imaging_And_Cancer_Therapy_Using_Lanthanide_Oxide_Nanoparticles_Current_Stat)  
 2 matches
- 
- [98]  [www.researchgate.net/publication/280866569\\_Increasing\\_the\\_sensitivity\\_of\\_NMR\\_diffusion\\_measurements\\_by\\_paramagnetic\\_longitudinal\\_relaxati](http://www.researchgate.net/publication/280866569_Increasing_the_sensitivity_of_NMR_diffusion_measurements_by_paramagnetic_longitudinal_relaxati)  
 3 matches
- 
- [99]  from a PlagScan document dated 2021-04-19 17:38  
 3 matches
- 
- [100]  Glutathione conjugated polyethylenimine on the surface of Fe3O4 magnetic nanoparticles as a theranostic agent for targeted and controlled curcumi  
 3 matches  
 1 documents with identical matches
- 
- [102]  [www.researchgate.net/publication/350056271\\_Low-energy\\_X-ray\\_attenuation\\_characteristics\\_of\\_Rhizophora\\_spp\\_composites](http://www.researchgate.net/publication/350056271_Low-energy_X-ray_attenuation_characteristics_of_Rhizophora_spp_composites)  
 2 matches
- 
- [103]  [www.researchgate.net/publication/350487358\\_Antioxidant\\_Cytotoxicity\\_and\\_Cytoprotective\\_Potential\\_of\\_Extracts\\_of\\_Grewia\\_Flava\\_and\\_Grewia](http://www.researchgate.net/publication/350487358_Antioxidant_Cytotoxicity_and_Cytoprotective_Potential_of_Extracts_of_Grewia_Flava_and_Grewia)  
 2 matches
- 
- [105]  from a PlagScan document dated 2019-03-14 02:30  
 1 matches
- 
- [106]  from a PlagScan document dated 2018-07-03 09:37  
 1 matches
- 
- [107]  from a PlagScan document dated 2020-12-11 14:01  
 2 matches
- 
- [110]  [pubs.rsc.org/en/content/articlehtml/2021/sc/d1sc02991f](http://pubs.rsc.org/en/content/articlehtml/2021/sc/d1sc02991f)  
 2 matches
- 
- [111]  "Comparative Analysis of Metal Ions and Texture of Ajwa Seed Powder Using Inductively Coupled Plasma–Mass Spectrometry.pdf" dated 2021-01-  
 2 matches
- 
- [112]  from a PlagScan document dated 2020-11-02 23:17  
 1 matches
-

19 pages, 4235 words

**PlagLevel: 4.0% selected / 15.1% overall**

111 matches from 113 sources, of which 20 are online sources.

#### **Settings**

Data policy: *Compare with web sources, Check against organization repository, Check against the Plagiarism Prevention Pool*

Sensitivity: *High*

Bibliography: *Bibliography excluded*

Citation detection: *Highlighting only*

Whitelist: --

# *Hydrothermally synthesized lanthanide-incorporated multi-functional zirconia nanoparticles: Potential candidate for multimodal imaging.*

Syed Mujtaba ul Hassan<sup>\*1</sup>, M. Tariq Siddique<sup>2</sup>, M. Fakhar-e-Alam<sup>3</sup>, M. Atif<sup>4</sup>, Adnan Saifullah<sup>2</sup>, Noreen Marwat<sup>5</sup>, Ahmat Khurshid<sup>2</sup>, Obaidullah Noor<sup>1</sup>, Nazia Hossain<sup>6</sup>, Shafiq Ahmad<sup>7</sup>, K. S. Alimgeer<sup>8</sup>

<sup>1</sup>*Department of Metallurgy & Materials Engineering (DMME), PIEAS, 45650, Islamabad, Pakistan*

<sup>2</sup>*Department of Physics & Applied Mathematics (DPAM), PIEAS, 45650, Islamabad, Pakistan*

<sup>3</sup>*Department of Physics, GC University 38000, Faisalabad*

<sup>4</sup>*Department of Physics and Astronomy, College of Science, King Saud University Riyadh 11451, Saudi Arabia*

<sup>5</sup>*Nuclear Medicine Oncology & Radiology Institute (NORI), Islamabad, Pakistan*

<sup>6</sup>*Civil and Infrastructure Engineering, School of Engineering, RMIT University, Melbourne, VIC 3001, Australia*

<sup>7</sup>*Industrial Engineering Department, College of Engineering, King Saud University, P.O. Box 800, Riyadh 11421, Saudi Arabia*

<sup>8</sup>*Department of Electrical and Computer Engineering, COMSATS University, Islamabad, Islamabad campus, Pakistan*

*\* Corresponding author: mujtaba@pieas.edu.pk; Tel. +92- 344-5524669*

Abstract:

### Objectives

Enabled zirconium oxide Nanoparticles (NPs) are multifunctional nanoparticles that can be employed for multimodal imaging and can show good biocompatibility.<sup>[10]</sup> In this work, we have synthesized Dysprosium (Dy) and Holmium (Ho) enabled zirconium oxide nanoparticles (Dy/Ho-ZrO<sub>2</sub> NPs) and have evaluated their potential as candidates for **contrast agents in different imaging modalities such as X-ray computed tomography (CT), Photoluminescence (PL) imaging and Magnetic Resonance Imaging (MRI)**. Rare earth elements have large atomic numbers, and their incorporation can enhance the X-ray attenuation characteristics of their host along with their optical properties. Rare earth elements exhibit paramagnetic character which can be utilized for MRI contrast enhancement. A combination of these imaging modalities can fulfill the limitations faced while using a single imaging technique.

### Methods

We have successfully synthesized Dy and Ho incorporated zirconia nanoparticles (Dy/Ho-ZrO<sub>2</sub>) by a simple one-step hydrothermal method.

### Results

Prepared NPs were characterized for their physical properties.<sup>[25]</sup> **X-ray diffraction (XRD) revealed the crystalline phases present in Dy-ZrO<sub>2</sub> and Ho-ZrO<sub>2</sub> NPs with a crystallite size of 27 nm and 21.54 nm respectively.** Scanning Electron Microscopy (SEM) results revealed the morphology of the nanoparticles, while EDS analysis gave the qualitative as well quantitative nature of synthesized nanocrystals. Photoluminescence (PL) data of Dy/Ho-Zirconia NPs have shown emission peaks near 419nm when excited at 310nm. Suspensions of prepared NPs with various concentrations were imaged on a CT machine in the clinical setting for contrast study. High CT contrast was observed for these NPs even at very low concentrations. Dysprosium doped sample was further evaluated for its potential as an MRI contrast agent. Dark cytotoxicity and photo-cytotoxicity results performed using Rhabdomyosarcoma (Rd) cancer cell lines revealed good biocompatibility of prepared NPs.

| Conclusions

*These results strongly signify the potential of these multifunctional Dy/Ho-Zirconia NPs to act as biocompatible multimodal imaging agents for biomedical applications.*

*Keywords: Multimodal imaging; Zirconia; Nanoparticles; Lanthanides*

## 1. Introduction

The development and synthesis of biocompatible, luminous bioimaging agents for use in diagnostics, imaging, and preventative medicine is critical for biomedicine's future (Mondal et al., 2020). Therefore, the development of nanomaterials suited for use as non-invasive diagnostic tools for biomedical purposes has attracted researchers' curiosity. The use of optically active components in conjunction with other imaging modalities is a particularly appealing technique to create multifunctional probes for biological imaging and identification (Li et al., 2016). The optical imaging method is particularly appealing for its high sensitivity, multicolor imaging, and activatable characteristic. However, its basic limitations are low spatial resolution and shallow tissue penetration (Pu et al., 2014).<sup>[10]</sup> To overcome this limitation, various imaging modalities such as magnetic resonance imaging and X-ray computed tomography imaging can be combined with optical imaging techniques (Cheng et al., 2014).<sup>[54]</sup> Because of its excellent spatial resolution and no tissue penetration limit, Computed Tomography (CT) has been widely employed as one of the most reliable imaging techniques (Lee et al., 2013). In terms of availability, efficiency, and affordability, CT has long been a standard technology in clinical imaging, and it can also provide high spatial and temporal resolution 3D structural details of tissues with differential X-ray absorption properties. CT imaging has long been utilized for bone imaging because it can easily discriminate between electron-dense structures (high-Z materials, such as bone) and electron-poor things (e.g., soft tissues). Magnetic resonance imaging (MRI), like CT, has an unlimited detection depth and can create 3D images, but it has a low detection sensitivity and lack multiplexing (James and Gambhir, 2012). However, MRI provides great resolution on soft tissues while CT excels at hard tissues thus MRI and CT are complimentary to each other.

Many currently accessible formulations involve potentially toxic ingredients, and clinical translation of nanotechnology will necessitate nanoparticles with the lowest feasible toxicity (Naahidi et al., 2013). Due to their good biocompatibility, ZrO<sub>2</sub> nanoparticles have been used in medical and orthopaedical applications, primarily for the repair and replacement of sick and damaged portions of the human skeleton, including bones, teeth, and joints (Wang et al., 2016). Hence, zirconium dioxide (ZrO<sub>2</sub>) may be employed as a host matrix for the design and manufacture of novel nanomaterials owing to its low toxicity. Moreover, the incorporation of inorganic nanoparticles with lanthanide ions is emerging as a promising class of new bio probes and has shown

great potential in various biomedical applications such as bio labeling, bioimaging, and theragnosis (Huang et al., 2019).  $Eu^{3+}$ ,  $La^{3+}$ ,  $Gd^{3+}$ ,  $Tb^{3+}$ ,  $Ce^{3+}$ , and other rare earth elements have been effectively incorporated within various host nanostructured systems for bioimaging applications (Graeve et al., 2010) (Doat et al., 2003). Lanthanide enabled NPs have displayed potential as multimodal imaging contrast agents as a result of their diverse yet tunable optical and magnetic properties (He et al., 2017). With the distinctive 4f manifold of trivalent lanthanide cations ( $Ln^{3+}$ ), Lanthanide enabled NPs upon excitation, emit light at different wavelengths ranging from the ultraviolet (UV) to near-infrared (NIR) regime (Liu et al., 2013).<sup>[59]</sup> The incorporation of lanthanides not only enhances the optical properties of inorganic metal oxides but also provides them with better thermal and photostability (Geitenbeek et al., 2019) (Chen et al., 2014). The high absorption coefficient for the host and low phonon energy ( $470\text{ cm}^{-1}$ ) of  $ZrO_2$  make it an ideal host for lanthanide ions (Liu et al., 2012). The inclusion of lanthanide can also enhance other important features of nanomaterials, such as magnetism and X-ray attenuation coefficient, which raises the potential of nanomaterials to be employed as contrast agents for multimodal imaging. Holmium and Dysprosium are among the elements having the highest magnetic moments, and they can generate significant transverse relaxation of hydrogen protons in free water. For ultra-high field  $T_2$  contrast agents, Ho and Dy based nanomaterials are the best options. MRI contrast agents based on high magnetic moment elements are projected to see considerable expansion in the near future, given the ongoing quest of ultra-high field intensity MRI.<sup>[16]</sup> The combination of photoluminescence, X-ray computed tomography, and magnetic resonance imaging is expected to provide high-resolution 3D details of tissues and cells with high sensitivity(Xing et al., 2012).

Herein, we have followed the hydrothermal route for synthesizing Dy and Ho incorporated zirconia NPs. Low crystallization temperatures enable direct production of nanocrystalline powders with a high degree of precipitation which reduces the content of metal ions in effluents as per environmental regulations, making hydrothermal synthesis a soft chemical route with significant advantages (Robert et al., 2005). Prepared nanoparticles were characterized for their physical properties and were first-ever evaluated for their bi-modal imaging potential by studying their PL, CT and MRI contrast properties.<sup>[10]</sup> Although bare zirconia NPs have been evaluated previously for their in-vitro cytotoxicity, however, the cytotoxicity of the enabled NPs should also be evaluated to estimate their full potential for biomedical applications. We have evaluated the dark cytotoxicity



of prepared nanoparticles on Rhabdomyosarcoma (Rd) cancer cells along with their photo-cytotoxicity using the MTT assay and red laser.

## 2. Materials and Methods

### 2.1. Chemicals and reagents

Research grade Zirconium chloride, Dysprosium oxide, Holmium oxide, Nitric acid, and Urea were purchased from Sigma Aldrich. Nitrates of Dy and Ho were obtained upon reacting their oxides with nitric acid. Other reagents used for dark cytotoxicity and phototoxicity include Minimum Essential Medium (MEM), Fetal Bovine Serum (FBS), Dimethyl sulfoxide (DMSO), Phosphate Buffered Saline (PBS), and Rd cell lines from the National Institute of Health (NIH).

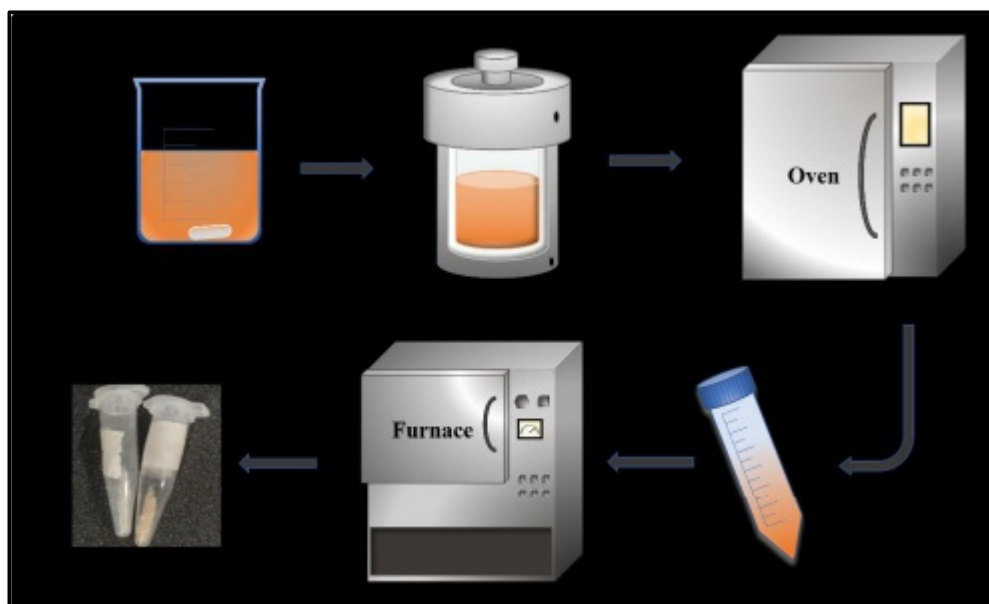


Figure 1. Schematics of Synthesis for Dy/Ho-Zirconia NPs.

### 2.2. Synthesis of Dy/Ho-ZrO<sub>2</sub> Nanoparticles

Schematics of the synthesis procedure are shown in Figure 1. Dy/Ho-ZrO<sub>2</sub> NPs were prepared by a hydrothermal method as reported previously for Eu doped ZrO<sub>2</sub> NPs (Atabaev, 2018). ZrCl<sub>4</sub> and Dy(NO<sub>3</sub>)<sub>3</sub>·6H<sub>2</sub>O were taken in mole ratios 0.89:0.11 and dissolved in 70ml deionized water in a beaker with vigorous magnetic stirring. 1.75g Urea was then added to the solution. After 20mins of stirring, the solution was transferred into a 100ml Teflon-lined stainless autoclave reactor which was then placed into a wind drying oven at 140°C for 2

hrs. Pressurized heating facilitated the production of fine Zirconia nanoparticles. The autoclave was allowed to cool down to room temperature. The white crystalline product was obtained upon opening the Teflon flask which was washed three times with deionized water by centrifuging at 6000rpm. Obtained 11% Dy-ZrO<sub>2</sub> nanoparticles were dried overnight at 65°C and were further calcinated for 1 hour and at 700°C. The same procedure was followed using Ho(NO<sub>3</sub>)<sub>3</sub>.5H<sub>2</sub>O in place of Dy(NO<sub>3</sub>)<sub>3</sub> to obtain 11% Ho-ZrO<sub>2</sub> NPs. The resulting nanoparticles when ultrasonicated for 10 minutes lead to homogenous suspension of nanoparticles in deionized water.

### 2.3. Characterization of Dy/Ho-ZrO<sub>2</sub>

Physical characterizations for the prepared nanoparticles were performed using powder X-Ray diffraction (Cu-Kα radiations, 0.154nm), Scanning electron microscopy, and Energy Dispersive X-ray spectroscopy. Tyndall test was performed to examine the colloidal stability of NPs (Stetefeld et al., 2016).<sup>[59]▶</sup> *The optical properties of the samples were studied using an F-98 fluorescence spectrometer. CT scans of synthesized samples were performed using General Electric's Discovery SPECT/CT at NORI hospital Islamabad. MRI contrast properties were studied using 1.5T GE MRI scanner. -Cell viability and phototoxicity test were conducted on Rd cancer cell lines. Absorbance data was recorded using a microplate reader. All bio characterizations were performed in a sterile environment.*

### 2.4. Cell culture and cell viability test

Human Rhabdomyosarcoma (Rd) cell lines representing the muscle cancer cell (Stevens et al., 2008)<sup>[89]▶</sup> were received from the National Institute of Health (NIH). Cells were sub-cultured in minimum essential medium (MEM) non-essential amino acids solution containing 10% Fetal Bovine Serum (FBS). Moist environment and 37°C temperature were provided for facilitating the growth and to ensure adequate adhesion to the substrate.<sup>[19]▶</sup> Upon achieving the confluence state, the cells were seeded in a 96 well plate and were placed in an incubator at 37°C for further growth and adhesion.<sup>[19]▶</sup> After 24 hours of subculturing, cells were treated with various concentrations (60-240µg/ml in FBS) of prepared nanoparticles and were further incubated for 24 hours.<sup>[19]▶</sup> Cell viability was determined by performing an MTT assay in a 96 well plate by a method as described in previous studies (AlSalhi et al., 2020; Atif et al., 2019, 2016, 2012, 2011b, 2011a, 2011c, 2010, 2009; Fakhar-E-Alam et al.,

2012; Fakhar-e-Alam et al., 2020; Iqbal et al., 2020; Hayat et al., 2013). All cell culture experiments were performed in a sterile environment inside a laminar flow hood.

### <sup>[38]</sup> 3. Results and discussion

Characteristic XRD peaks of Dy-ZrO<sub>2</sub> and Ho-ZrO<sub>2</sub> can be seen in the spectrum as shown in figure 2. Spectrum was analyzed and peaks were found to agree with the reported literature (Atabaev, 2018). Peaks for the Dy-ZrO<sub>2</sub> were indexed using ICDD card number 96-900-7449. XRD Peaks of the Ho-ZrO<sub>2</sub> sample were indexed using ICDD card number 96-152-5707 and both the samples were found to be in a tetragonal phase with excellent crystallinity. The crystallite size ( $\tau$ ) for both samples was calculated using Scherrer's formula.

$$\tau = \frac{K\lambda}{\beta \cos\theta}$$

Where  $K$  is the shape factor,  $\lambda$  is the wavelength of X-rays,  $\beta$  is the full width at half the maximum intensity and  $\theta$  is the Bragg angle. Dy-ZrO<sub>2</sub> possessed a crystallite size of 27nm while that for Ho-ZrO<sub>2</sub> was 21.54nm.

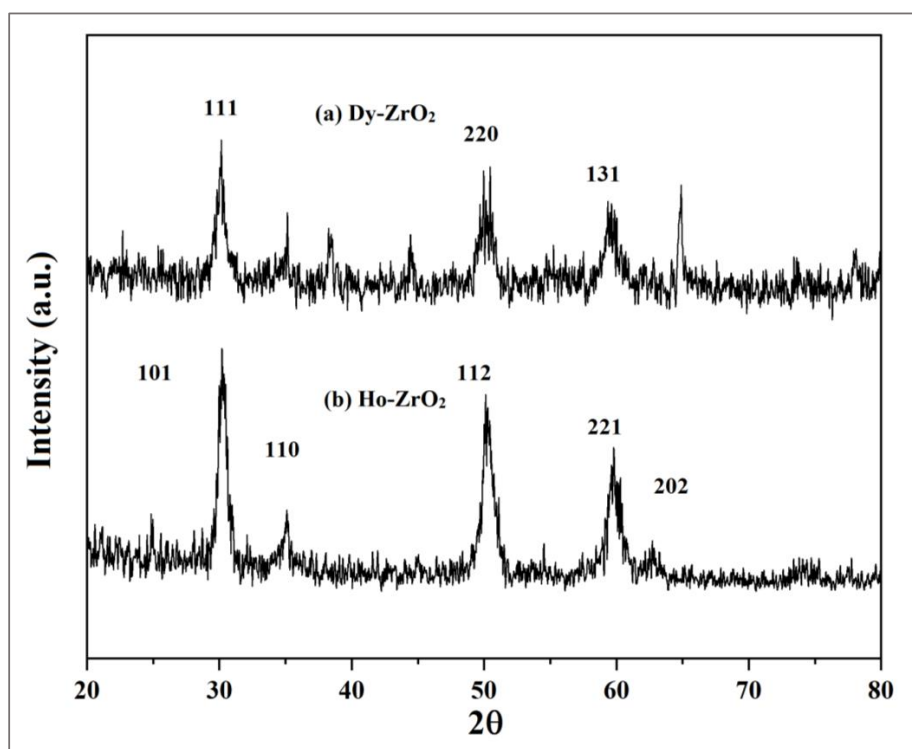


Figure 2. XRD analysis of 11% Dy/Ho-Zirconia Samples.

SEM for both samples was performed for high-resolution imaging while EDX was performed to study the elemental composition as shown in figure three. EDS results confirmed the successful incorporation of Dy and Ho atoms into vacant sites of tetragonal zirconia crystals was the prerequisite for contrast experiments.

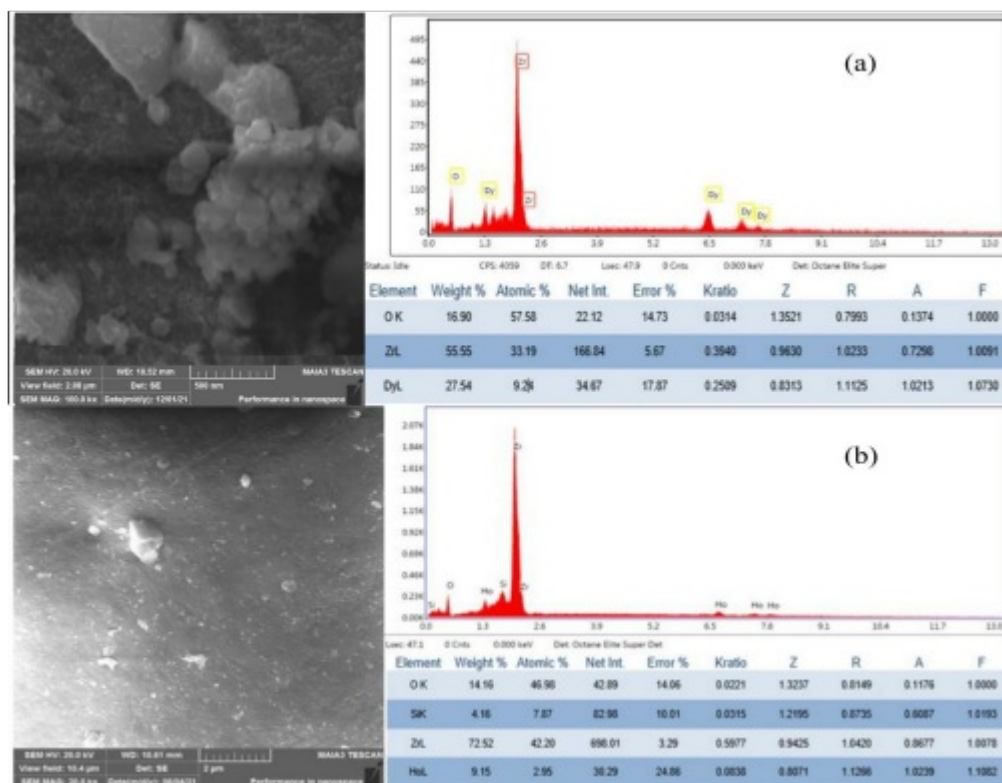


Figure 3. SEM micrograph and EDX results for (a) Dy-ZnO<sub>2</sub> and (b) Ho-ZrO<sub>2</sub>.

Uniform suspension of synthesized nanoparticles in an appropriate medium is very important for biomedical applications and contrast studies. To determine the colloidal stability Tyndall test was performed using a red laser as shown in figure 4(b). The suspension of NPs was exposed to a red laser at varying time intervals up to 30 h and the results indicate good colloidal stability of nanoparticles over an extended period.

### 3.1. Photoluminescence, ~~and~~ CT contrast and MRI contrast Study

Optical characteristics were evaluated using an F-98 fluorescence spectrophotometer. Emission wavelength scan shows the photoluminescence spectra of Dy and Ho enabled zirconia nanoparticles recorded in the

range of 400 nm-560 nm is shown in figure 4 (a). Both samples show a prominent and intense emissions spectrum near 419 nm when excited at the wavelength of 310 nm.

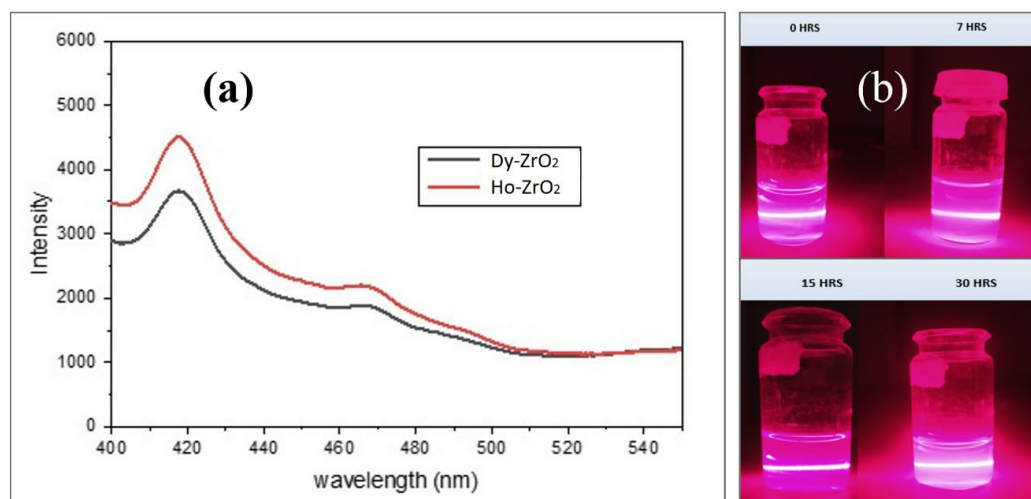


Figure 4. (a) PL Spectra of Dy/Ho-ZrO<sub>2</sub> at an excitation wavelength of 310nm; (b) Tyndall test with a red laser (630nm) at subsequent time intervals.

CT scans of the suspensions of Dy/Ho-ZrO<sub>2</sub> NPs in a water phantom were performed at three different energies 80 KV, 100 KV, and 120 KV as shown in Figure 5. These energies are normally used for patient scans in clinical settings. Contrast materials present in glass vials were placed in a water-filled phantom. Different concentrations of contrast material ( 0,2.1,2.8,4.2,6.3 and 7mg/ml) were scanned at three energies while the rest of the parameters were similar. Contrast (Hounsfield units) is decreasing with increasing energy as shown in figure 5.

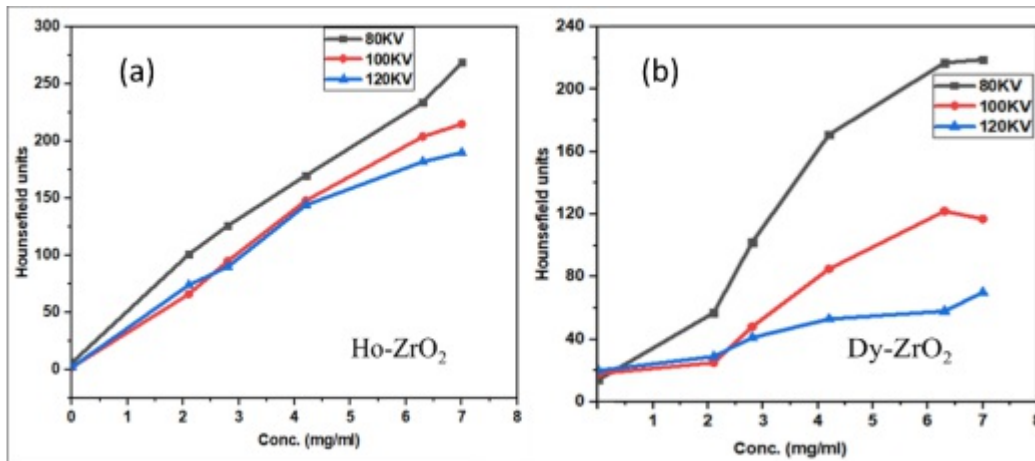
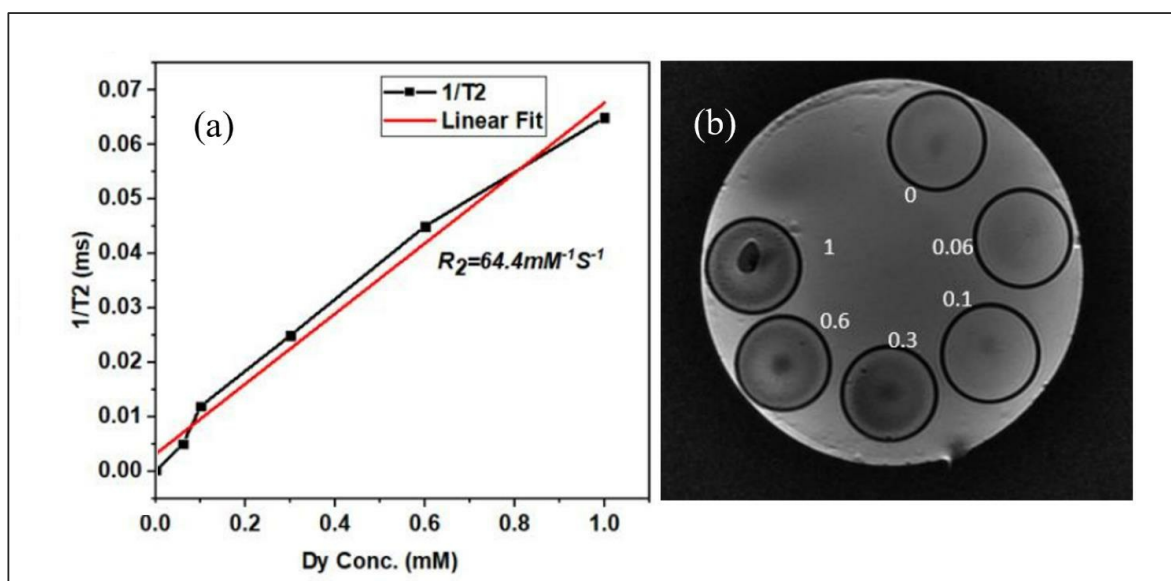


Figure 5. The plot of HU vs Different concentrations of prepared samples at three different energies.

(a) for Ho-ZrO<sub>2</sub>; (b) for Dy-ZrO<sub>2</sub>

As energy is increased, more and more photons are passing through the material without making any interaction as a cross-section for photoelectric, and Compton's effect is low at high energies. Also, increasing behavior of the X-ray attenuation coefficient can be observed with the concentration of the NPs. The highest X-ray attenuation i.e. high contrast was observed at 80 KV while the lowest contrast was at 120 KV.<sup>[5]</sup> These optical and X-ray attenuation results indicate the superior potential of Dy/Ho=ZrO<sub>2</sub> NPs to be used as CT contrast agents.

For the study of MRI contrast properties, a 1.5T GE MRI scanner was used. Inside a cylindrical water-filled phantom, a series of Dy-ZrO<sub>2</sub> samples with varying Dysprosium ion concentrations were placed. The water phantom was placed inside the scanner using the knee flex coil. Scans were taken using the Fast Spin Echo (FSE) sequence. T<sub>2</sub> weighted scans were conducted since Dysprosium increase the T<sub>2</sub> relaxation rate. The recovery time TR was set to 3000ms, and the echo times TE were 50ms, 90ms, 130ms, 170ms, 190ms, 500ms, and 900ms, respectively. The slice thickness was 3.5mm, and the length of the eco train was 35.<sup>[31]</sup> The results were presented as a series of DICOM images. IMAGEJ software was used to open DICOM images. The appropriate Region of Interest (ROI) was chosen, and the intensity variation with echo time was recorded. T<sub>2</sub> time for a specific ROI or vial was calculated using a plot of intensity versus echo time and an exponential curve fit. T<sub>2</sub> time for the remaining vials was computed in the same way. Finally, T<sub>2</sub> durations were plotted against the concentration of paramagnetic ions, yielding a relaxation rate in mM<sup>-1</sup>s<sup>-1</sup>.



*Figure 6. (a) Plot of  $1/T_2$  time vs  $Dy^{3+}$  ion concentration; (b) Contrast vials placed in water medium having concentration 0 to 1mM Dy concentration.*

*The  $T_2$  weighted images become darker due to a high concentration of paramagnetic ions. In order to depict clinical conditions, contrast vials were placed in a deionized water medium. Relaxivity rate  $R_2$  in units of  $mM^{-1}S^{-1}$  is obtained by plotting  $1/T_2$  times against Dy concentration. The  $R_2$  value obtained after the linear fit is  $64.4 mM^{-1}s^{-1}$  as shown in figure 6, which is close to values obtained by Tirusew Tegafaw et al (Tegafaw et al., 2015).*

### *3.2. Dark cytotoxicity and Photo-cytotoxicity studies.*

*MTT Assay and phototoxicity studies were performed after treating the cells with Dy/Ho-ZrO<sub>2</sub> NPs. The viability of RD cells, incubated with increasing concentrations of the NPs (60  $\mu$ g/ml to 240  $\mu$ g/ml) was evaluated using the MTT colorimetric assay. Culture media was replaced with 100  $\mu$ L PBS solution containing 20  $\mu$ L MTT stock solution (5.0 mg/mL) and cells were further incubated for 4 hrs. The MTT working solution was then aspirated and 100  $\mu$ L of DMSO was added per well to solubilize the formazan crystals formed within the viable cells. The absorbance data was recorded using a microplate reader. The percentage of cell viability was determined from the absorbance data using the following relation.<sup>[10]</sup>*

$$\text{Cell viability percentage} = \frac{\text{Treated cells absorbance}}{\text{Untreated cells absorbance}} \times 100$$



Cell viability was found to be 88% or more even at higher concentrations up to 240µg/ml while much better cell viability was observed at low concentrations which is indicative of very less dark cytotoxicity of these NPs as shown in figure 7.

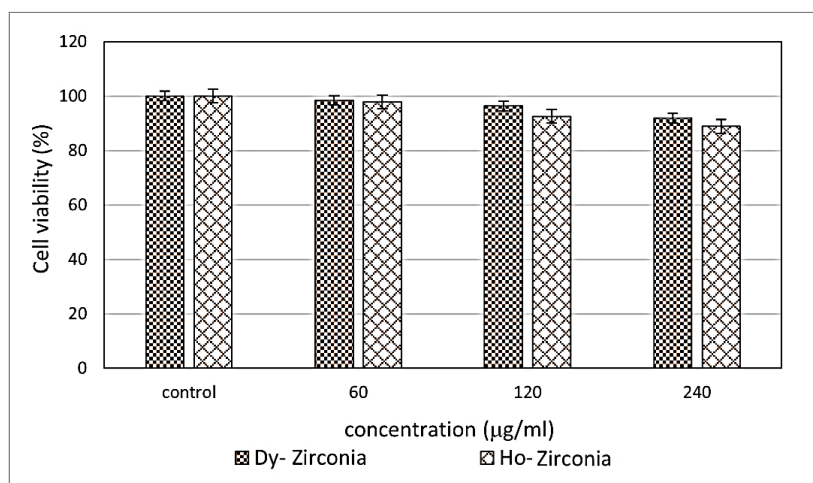


Figure 7. MTT Assay cytotoxicity Results.

For phototoxicity cells were exposed to different doses of red laser after 24 hours of treatment with NPs. Cells were further incubated for 24 hours before performing MTT assay. The data of phototoxicity at a fixed dose of 60 µg/ml is plotted against varying doses of light as shown in figure 8.<sup>[12]</sup> Cell viability for both samples was found to be more than 80% even at higher light doses which indicates the low phototoxicity of these samples.



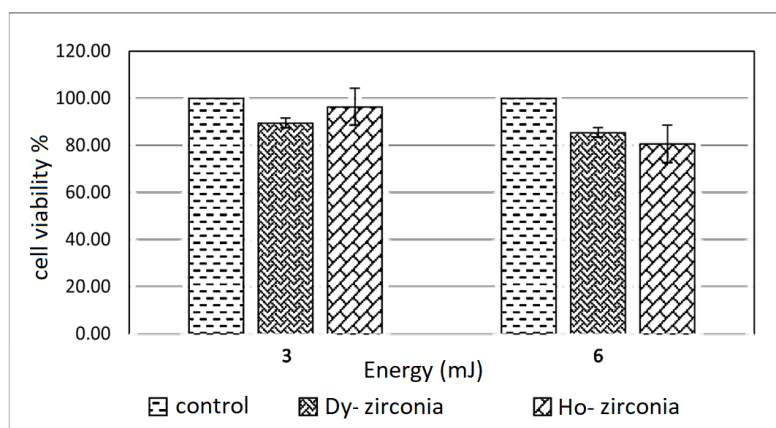


Figure 8. Phototoxicity results, both samples have a concentration of 60 $\mu$ g/ml.

#### 4. Conclusion

Rare earth metals Dysprosium and Holmium were used to synthesize lanthanide-incorporated zirconia nanoparticles via the hydrothermal method. Conventional characterizations like XRD, SEM revealed the crystalline nature and morphologies of the Dy/Ho-ZrO<sub>2</sub> NPs. Tyndall test shows good colloidal stability of these NPs. Dark cytotoxicity and phototoxicity studies of the samples have revealed their nontoxic behavior. Optical properties, X-ray attenuation and MRI relaxivity characteristics signify the potential of these nanoparticles to be used for multimodal imaging i.e., PL/CT/MRI imaging technique. The use of PL, MRI, and CT together can produce medical images with excellent resolution, sensitivity, and information for medical diagnosis with no limit on the target sites detection depth.

*Acknowledgments: Researchers Supporting Project number (RSP-2021/397), King Saud University, Riyadh, Saudi Arabia.*

*Conflicts of Interest: The authors declare that they have no known competing financial interests or personal relationships that could have appeared to influence the work reported in this paper.*

## References

- AlSalhi, M.S., Aziz, M.H., Atif, M., Fatima, M., Shaheen, F., Devanesan, S., Aslam Farooq, W., 2020. Synthesis of NiO nanoparticles and their evaluation for photodynamic therapy against HeLa cancer cells. *J. King Saud Univ. - Sci.* 32. <https://doi.org/10.1016/j.jksus.2019.11.033>
- Atabaev, S., 2018. Fabrication and optical properties of Eu-doped zirconia nanoparticles. *Mater. Today Proc.* 6, 7–10. <https://doi.org/10.1016/j.matpr.2018.05.068>
- Atif, M., AlSalhi, M.S., AlObiadi, A.A., Aldwayyan, A.S., 2012. Fluorescence spectra of cultured normal and malignant lung cells. *Laser Phys.* 22. <https://doi.org/10.1134/S1054660X1208004X>
- Atif, M., Fakhar-E-Alam, M., Abbas, N., Siddiqui, M.A., Ansari, A.A., Al-Khedhairi, A.A., Wang, Z.M., 2016. In Vitro Cytotoxicity of Mesoporous SiO<sub>2</sub>@Eu(OH)<sub>3</sub> Core-Shell Nanospheres in MCF-7. *J. Nanomater.* 2016. <https://doi.org/10.1155/2016/7691861>
- Atif, M., Fakhar-E-Alam, M., AlSalhi, M.S., 2011a. Role of sensitivity of zinc oxide nanorods (ZnO-NRs) based photosensitizers in hepatocellular site of biological tissue. *Laser Phys.* 21. <https://doi.org/10.1134/S1054660X11190029>
- Atif, M., Fakhar-E-Alam, M., Firdous, S., Zaidi, S.S.Z., Suleman, R., Ikram, M., 2010. Study of the efficacy of 5-ALA mediated photodynamic therapy on human rhabdomyosarcoma cell line (RD). *Laser Phys. Lett.* 7. <https://doi.org/10.1002/lapl.201010061>
- Atif, M., Fakhar-E-Alam, M., Zaidi, S.S.Z., Suleman, R., 2011b. Study of the efficacy of Photofrin®-mediated PDT on human hepatocellular carcinoma (HepG2) cell line. *Laser Phys.* 21. <https://doi.org/10.1134/S1054660X11110028>
- Atif, M., Firdous, S., Khurshid, A., Noreen, L., Zaidi, S.S.Z., Ikram, M., 2009. In vitro study of 5-aminolevulinic acid-based photodynamic therapy for apoptosis in human cervical HeLa cell line. *Laser Phys. Lett.* 6. <https://doi.org/10.1002/lapl.200910087>
- Atif, M., Firdous, S., Mahmood, R., Fakhar-E-Alam, M., Zaidi, S.S.Z., Suleman, R., Ikram, M., Nawaz, M., 2011c. Cytotoxic and photocytotoxic effect of Photofrin® on human laryngeal carcinoma (Hep2c) cell line. *Laser Phys.* 21. <https://doi.org/10.1134/S1054660X11130020>

- Atif, M., Iqbal, S., Fakhar-E-Alam, M., Ismail, M., Mansoor, Q., Mughal, L., Aziz, M.H., Hanif, A., Farooq, W.A., 2019. Manganese-Doped Cerium Oxide Nanocomposite Induced Photodynamic Therapy in MCF-7 Cancer Cells and Antibacterial Activity. *Biomed Res. Int.* 2019. <https://doi.org/10.1155/2019/7156828>
- Chen, G., Qiu, H., Prasad, P.N., Chen, X., 2014. Upconversion nanoparticles: Design, nanochemistry, and applications in Theranostics. *Chem. Rev.* 114, 5161–5214. <https://doi.org/10.1021/cr400425h>
- Cheng, L., Liu, J., Gu, X., Gong, H., Shi, X., Liu, T., Wang, C., Wang, X., Liu, G., Xing, H., Bu, W., Sun, B., Liu, Z., 2014. PEGylated WS<sub>2</sub> nanosheets as a multifunctional theranostic agent for in vivo dual-modal CT/photoacoustic imaging guided photothermal therapy. *Adv. Mater.* 26, 1886–1893. <https://doi.org/10.1002/adma.201304497>
- Doat, A., Fanjul, M., Pellé, F., Hollande, E., Lebugle, A., 2003. Europium-doped bioapatite: A new photostable biological probe, internalizable by human cells. *Biomaterials* 24, 3365–3371. [https://doi.org/10.1016/S0142-9612\(03\)00169-8](https://doi.org/10.1016/S0142-9612(03)00169-8)
- Fakhar-E-Alam, M., Ali, S.M.U., Ibupoto, Z.H., Kimleang, K., Atif, M., Kashif, M., Loong, F.K., Hashim, U., Willander, M., 2012. Sensitivity of A-549 human lung cancer cells to nanoporous zinc oxide conjugated with Photofrin. *Lasers Med. Sci.* 27. <https://doi.org/10.1007/s10103-011-0989-8>
- Fakhar-e-Alam, M., Aqrab-ul-Ahmad, Atif, M., Alimgeer, K.S., Suleman Rana, M., Yaqub, N., Aslam Farooq, W., Ahmad, H., 2020. Synergistic effect of TEMPO-coated TiO<sub>2</sub> nanorods for PDT applications in MCF-7 cell line model. *Saudi J. Biol. Sci.* <https://doi.org/10.1016/j.sjbs.2020.09.027>
- Geitenbeek, R.G., Salzmann, B.B.V., Nieuwelink, A.E., Meijerink, A., Weckhuysen, B.M., 2019. Chemically and thermally stable lanthanide-doped Y<sub>2</sub>O<sub>3</sub> nanoparticles for remote temperature sensing in catalytic environments. *Chem. Eng. Sci.* 198, 235–240. <https://doi.org/10.1016/j.ces.2018.10.004>
- Graeve, O.A., Kanakala, R., Madadi, A., Williams, B.C., Glass, K.C., 2010. Luminescence variations in hydroxyapatites doped with Eu<sup>2+</sup> and Eu<sup>3+</sup> ions. *Biomaterials* 31, 4259–4267.

<https://doi.org/10.1016/j.biomaterials.2010.02.009>

Hayat, K., Khurshid, A., Rafiq, M.A., Durrani, S.K., Zaidi, S.S.Z., Ikram, M., Hasan, M.M., 2013. The potential of PEGylated BaMnO<sub>3</sub> nanoparticles as drug delivery agents. *Laser Phys. Lett.* 10. <https://doi.org/10.1088/1612-2011/10/2/025603>

He, S., Johnson, N.J.J., Nguyen Huu, V.A., Cory, E., Huang, Y., Sah, R.L., Jokerst, J. V., Almutairi, A., 2017. Simultaneous enhancement of photoluminescence, MRI Relaxivity, and CT contrast by tuning the interfacial layer of lanthanide heteroepitaxial nanoparticles. *Nano Lett.* 17, 4873–4880. <https://doi.org/10.1021/acs.nanolett.7b01753>

Huang, P., Zheng, W., Gong, Z., You, W., Wei, J., Chen, X., 2019. Rare earth ion- and transition metal ion-doped inorganic luminescent nanocrystals: from fundamentals to biodetection. *Mater. Today Nano.* <https://doi.org/10.1016/j.mtnano.2019.100031>

Iqbal, S., Fakhar-e-Alam, M., Atif, M., Amin, N., Ali, A., Shafiq, M., Ismail, M., Hanif, A., Farooq, W.A., 2020. Photodynamic therapy, facile synthesis, and effect of sintering temperature on the structure, morphology, optical properties, and anticancer activity of Co<sub>3</sub>O<sub>4</sub> nanocrystalline materials in the HepG2 cell line. *J. Photochem. Photobiol. A Chem.* 386. <https://doi.org/10.1016/j.jphotochem.2019.112130>

James, M.L., Gambhir, S.S., 2012. A MOLECULAR IMAGING PRIMER : MODALITIES , IMAGING AGENTS , AND APPLICATIONS MOLECULAR IMAGING AGENTS APPLICATIONS OF MOLECULAR IMAGING GUIDE TO PERFORMING A MOLECULAR ... 897–965. <https://doi.org/10.1152/physrev.00049.2010>

Lee, N., Choi, S.H., Hyeon, T., 2013. Nano-sized CT contrast agents. *Adv. Mater.* 25, 2641–2660. <https://doi.org/10.1002/adma.201300081>

Li, X., Zhang, X.N., Li, X.D., Chang, J., 2016. Multimodality imaging in nanomedicine and nanotheranostics.

*Cancer Biol. Med.* <https://doi.org/10.20892/j.issn.2095-3941.2016.0055>

Liu, Y., Tu, D., Zhu, H., Chen, X., 2013. Lanthanide-doped luminescent nanoprobes: Controlled synthesis, optical spectroscopy, and bioapplications. *Chem. Soc. Rev.* 42, 6924–6958. <https://doi.org/10.1039/c3cs60060b>

Liu, Y., Zhou, S., Tu, D., Chen, Z., Huang, M., Zhu, H., Ma, E., Chen, X., 2012. Amine-functionalized lanthanide-doped zirconia nanoparticles: Optical spectroscopy, time-resolved fluorescence resonance energy transfer biodetection, and targeted imaging. *J. Am. Chem. Soc.* <https://doi.org/10.1021/ja306066a>

Mondal, S., Nguyen, V.T., Park, S., Choi, J., Thien Vo, T.M., Shin, J.H., Kang, Y.H., Oh, J., 2020. Rare earth element doped hydroxyapatite luminescent bioceramics contrast agent for enhanced biomedical imaging and therapeutic applications. *Ceram. Int.* 46, 29249–29260. <https://doi.org/10.1016/j.ceramint.2020.08.099>

Naahidi, S., Jafari, M., Edalat, F., Raymond, K., Khademhosseini, A., Chen, P., 2013. Biocompatibility of engineered nanoparticles for drug delivery. *J. Control. Release.* <https://doi.org/10.1016/j.jconrel.2012.12.013>

Pu, K., Shuhendler, A.J., Jokerst, J. V., Mei, J., Gambhir, S.S., Bao, Z., Rao, J., 2014. Semiconducting polymer nanoparticles as photoacoustic molecular imaging probes in living mice. *Nat. Nanotechnol.* 9, 233–239. <https://doi.org/10.1038/nnano.2013.302>

Stetefeld, J., McKenna, S.A., Patel, T.R., 2016. Dynamic light scattering: a practical guide and applications in biomedical sciences. *Biophys. Rev.* 8, 409–427. <https://doi.org/10.1007/s12551-016-0218-6>

Stevens, M., Frobisher, C., Hawkins, M., Jenney, M., Lancashire, E., Reulen, R., Taylor, A., Winter, D., 2008. *The British Childhood Cancer Survivor Study: Objectives, methods, population structure, response rates*

and initial descriptive information. *Pediatr. Blood Cancer* 50, 1018–1025. <https://doi.org/10.1002/pbc>

Tegafaw, T., Xu, W., Ahmad, M.W., Baeck, J.S., Chang, Y., Bae, J.E., Chae, K.S., Kim, T.J., Lee, G.H., 2015.

*Dual-mode T1 and T2 magnetic resonance imaging contrast agent based on ultrasmall mixed gadolinium-dysprosium oxide nanoparticles: Synthesis, characterization, and in vivo application. Nanotechnology* 26, 365102. <https://doi.org/10.1088/0957-4484/26/36/365102>

Wang, J., Yin, W., He, X., Wang, Q., Guo, M., Chen, S., 2016. *Good Biocompatibility and Sintering Properties of Zirconia Nanoparticles Synthesized via Vapor-phase Hydrolysis. Sci. Rep.* 6, 1–9. <https://doi.org/10.1038/srep35020>

Xing, H., Bu, W., Zhang, S., Zheng, X., Li, M., Chen, F., He, Q., Zhou, L., Peng, W., Hua, Y., Shi, J., 2012.

*Multifunctional nanoprobes for upconversion fluorescence, MR and CT trimodal imaging. Biomaterials* 33, 1079–1089. <https://doi.org/10.1016/j.biomaterials.2011.10.039>